

DEEP LEARNING OF PARAMETERIZED EQUATIONS WITH APPLICATIONS TO UNCERTAINTY QUANTIFICATION

TONG QIN*, ZHEN CHEN*, JOHN D. JAKEMAN*, AND DONGBIN XIU†

Abstract. We propose a numerical method for discovering unknown parameterized dynamical systems by using observational data of the state variables. Our method is built upon and extends the recent work of discovering unknown dynamical systems, in particular those using deep neural network (DNN). We propose a DNN structure, largely based upon the residual network (ResNet), to not only learn the unknown form of the governing equation but also take into account the random effect embedded in the system, which is generated by the random parameters. Once the DNN model is successfully constructed, it is able to produce system prediction over longer term and for arbitrary parameter values. For uncertainty quantification, it allows us to conduct uncertainty analysis by evaluating solution statistics over the parameter space.

Key words. Deep neural network, residual network, uncertainty quantification.

1. Introduction. The ability to construct predictive models from data is essential to most if not all quantitative scientific and engineering disciplines. A significant amount of research has been conducted in this direction. Early efforts include symbolic regression ([2, 34]), equation-free modeling [17], heterogeneous multi-scale method (HMM) ([8]), artificial neural networks ([12]), nonlinear regression ([43]), empirical dynamic modeling ([39, 50]), nonlinear Laplacian spectral analysis ([11]), automated inference of dynamics ([35, 6, 7]), etc. More recent effort cast the problem as one of function approximation problems and employ data-driven approaches to resolve it. The unknown governing equations are treated as target functions, which map state variables to their time derivatives. One popular approach is to employ sparsity-promoting algorithms, such as the least absolute shrinkage and selection operator (LASSO) [40], to select basis functions from a large dictionary set, which contains all candidate models, see for example [4, 41]. Numerous other approaches have also been developed such as those based upon projection into polynomial spaces [46, 45], dynamic mode decomposition [33], operator inference [24], model selection approach [23], and Gaussian process regression [28].

Recent progress in machine learning, especially in deep neural networks (DNN), has provided new perspectives to data-driven modeling. Approaches such as physics informed neural networks [28, 27], PDE-net [22, 20], DNN with Runge-Kutta or multi-step integrator structures [29, 32], etc. aim at recovering hidden models in differential equation forms. Different network structures and properties are explored in the context of recovering ODE systems [32, 29, 26] and PDEs ([21, 22, 47]). DNNs have been used in other aspects of scientific computing. These include, construction of reduced order models [15], aiding numerical solvers of conservation laws ([30, 31]), approximation of Koopman operator ([3]), solving differential equations [19, 13, 44, 37], etc. For uncertainty quantification (UQ), DNNs were employed to approximate mappings from random parameters to quantities of interest (QoI) in [42]; incorporated in Bayesian framework and used as surrogate models [51, 52]; adopted to approximate distribution of QoI [49], etc.

*Optimization and Uncertainty Quantification Department, Sandia National Laboratory, Albuquerque, NM, 87123 USA (Email: jdjakeman@sandia.gov).

†Department of Mathematics, The Ohio State University, Columbus, OH 43210, USA. (Emails: qin.428@osu.edu, chen.7168@osu.edu, xiu.16@osu.edu). Funding: This work was partially supported by AFOSR FA9550-18-1-0102.

The focus of this paper is on recovery of unknown parameterized dynamical systems. That is, not only is the form of the governing equations unknown, the system also possesses parameters that are unknown. Systems with unknown/uncertain parameters are often studied in the context of uncertainty quantification (UQ). When the governing equations are known, various standard UQ techniques, e.g, those based on generalized polynomial chaos [10, 48], can be readily applied. These techniques are obviously not applicable when the governing equations are unavailable. In this paper, we proposed a data driven method that uses observation data of the state variables to recover unknown governing equations with embedded unknown/uncertain parameters. Our method is based on and extends the work of [26]. In [26], residual network (ResNet) ([14]) was used to recover unknown *deterministic* dynamical systems. This paper extends the approach to unknown stochastic/random dynamical systems. To accomplish this, we introduce additional inputs in the DNN structure to incorporate the unknown system parameters, as well as an input for “time step”. The proposed DNN is thus able to register system responses with respect to different system parameters. This in turn allows us to create DNN model for the evolution of the underlying unknown equations. The introduction of the time-step input allows the network to incorporate measurement data over non-uniform time levels. This adds more flexibility in the DNN modeling construction. It also allows us to conduct system prediction using different time steps. Note that our DNN modeling utilizes approximation of the flow map of the unknown system. This was proposed in [26] and is different from many other recovery methods. This flow-map approach has two advantages: (i) the approximation is based exact time integration and induces no temporal error associated with time step; (ii) temporal numerical derivatives of the observational data, which are usually sensitive to noises, are not required.

Once the DNN models are successfully constructed, they allow us to conduct system predictions over longer term. More importantly, the proposed method is able to explore the parameter space and create model prediction at arbitrary parameter values. Uncertainty quantification of the unknown system thus becomes a post-process, as we can conduct UQ on the recovered DNN model using proper sampling methods. To this end, we also conduct some theoretical analysis to quantify the numerical errors in such UQ prediction.

2. Setup and Preliminaries. Let us consider a parameterized system

$$\frac{d}{dt}\mathbf{x}(t; \boldsymbol{\alpha}) = \mathbf{f}(\mathbf{x}, \boldsymbol{\alpha}), \quad \mathbf{x}(0) = \mathbf{x}_0, \quad (2.1)$$

where $\mathbf{x} = (x_1, \dots, x_d) \in I_{\mathbf{x}} \subseteq \mathbb{R}^d$ are state variables and $\boldsymbol{\alpha} = (\alpha_1, \dots, \alpha_\ell) \in I_{\boldsymbol{\alpha}} \subseteq \mathbb{R}^\ell$ are system parameters. We are interested in the solution behavior with respect to varying parameters. In the context of uncertainty quantification (UQ), which is a major focus of this paper, the parameters are equipped with a probability measure over $I_{\boldsymbol{\alpha}}$. We are interested in understanding the various solution statistics with respect to the input $\boldsymbol{\alpha}$.

The basic assumption of this paper is that the form of the governing equations (2.1), which manifests itself via the right-hand-side $\mathbf{f}(\mathbf{x}, \boldsymbol{\alpha}) : \mathbb{R}^d \times \mathbb{R}^\ell \rightarrow \mathbb{R}^d$, is unknown. Our goal is to create an accurate numerical model for the governing equation using data of the state variable \mathbf{x} . Although similar to the setting of the recent work of discovering unknown dynamical systems [26], our setting here represents a non-trivial extension. That is, not only the form of the right-hand-side \mathbf{f} is unknown, its associated parameters $\boldsymbol{\alpha}$ are also unknown.

2.1. Data. In order to learn the governing equation, we assume trajectory data of the state variables \mathbf{x} are available. More specifically, let N_T be the total number of trajectories. For each i -th trajectory, we have data in the following form,

$$\mathbf{X}^{(i)} = \left\{ \mathbf{x} \left(t_k^{(i)}; \boldsymbol{\alpha}^{(i)}, \mathbf{x}_0^{(i)} \right) \right\}, \quad i = 1, \dots, N_T, \quad k = 0, \dots, K^{(i)},$$

where $\{t_k^{(i)}\}$ are the time instances where the data are made available, and the parameter $\boldsymbol{\alpha}^{(i)}$ and the initial condition $\mathbf{x}_0^{(i)}$ associated with the i -th trajectory are unknown.

A distinct feature of the learning method in this paper is to approximate the underlying flow map of the unknown governing equation (2.1). The method requires the use of trajectory data from two different time instances. Consequently, we reorganize the data set into pairs of two adjacent time instances, for each $i = 1, \dots, N_T$,

$$\left\{ \mathbf{x} \left(t_k^{(i)}; \boldsymbol{\alpha}^{(i)}, \mathbf{x}_0^{(i)} \right), \quad \mathbf{x} \left(t_{k+1}^{(i)}; \boldsymbol{\alpha}^{(i)}, \mathbf{x}_0^{(i)} \right) \right\}, \quad k = 0, \dots, K^{(i)} - 1.$$

Note that for the autonomous system (2.1) considered in this paper, only the time difference is important in the pairs. The actual time value is not relevant for it can be arbitrarily shifted. Therefore, we write the data pairs as, for each $i = 1, \dots, N_T$,

$$\left\{ \mathbf{x} \left(0; \boldsymbol{\alpha}^{(i)}, \mathbf{x}_0^{(i)} \right), \quad \mathbf{x} \left(\Delta_k^{(i)}; \boldsymbol{\alpha}^{(i)}, \mathbf{x}_0^{(i)} \right) \right\}, \quad k = 0, \dots, K^{(i)} - 1,$$

where $\Delta_k^{(i)} = t_{k+1}^{(i)} - t_k^{(i)}$. Finally, to account for possible noises in the data and by using a single index to simplify notation, we write the data set as

$$S = \left\{ \mathbf{z}_j^{(1)}, \mathbf{z}_j^{(2)} \right\}, \quad j = 1, \dots, J, \quad (2.2)$$

where $J = K^{(1)} + \dots + K^{(N_T)}$ is the total number of data pairs and

$$\mathbf{z}_j^{(1)} = \left(\mathbf{x} \left(0; \boldsymbol{\alpha}^{(j)}, \mathbf{x}_0^{(j)} \right) + \epsilon_j^{(1)}, \boldsymbol{\alpha}^{(j)}, \Delta_j \right) \quad \mathbf{z}_j^{(2)} = \mathbf{x} \left(\Delta_j; \boldsymbol{\alpha}^{(j)}, \mathbf{x}_0^{(j)} \right) + \epsilon_j^{(2)}, \quad (2.3)$$

where $\epsilon_j^{(1)}$ and $\epsilon_j^{(2)}$ are noises/errors in the state variable data. That is, each j -th pair, $j = 1, \dots, J$, consists of data of the state variables \mathbf{x} separated by a time difference Δ_j . The pair resides on a certain trajectory associated with an unknown parameter value $\boldsymbol{\alpha}^{(j)}$ and is originated from an unknown initial condition $\mathbf{x}_0^{(j)}$. We also define

$$I_\Delta = [\min_j \Delta_j, \max_j \Delta_j] \quad (2.4)$$

to be the range of the time lags in the dataset (2.2).

2.2. Deep neural networks. In this paper we adopt deep neural network (DNN) as the primary modeling method for recovering unknown governing equation. In particular, we employ feed forward neural networks (FNN) as the core building block. A standard FNN defines a nonlinear map in the following sense. Let $\mathbf{N} : \mathbb{R}^m \rightarrow \mathbb{R}^n$ be the operator associated with a FNN with $M \geq 1$ hidden layers. Its map can be written as

$$\mathbf{y}^{out} = \mathbf{N}(\mathbf{y}^{in}; \Theta) = \mathbf{W}_{M+1} \circ (\sigma_M \circ \mathbf{W}_M) \circ \dots \circ (\sigma_1 \circ \mathbf{W}_1)(\mathbf{y}^{in}), \quad (2.5)$$

where \mathbf{W}_j is weight matrix between the j -th layer and the $(j + 1)$ -th layer, $\sigma_j : \mathbb{R} \rightarrow \mathbb{R}$ is the activation function, and \circ stands for operator composition. Following the standard notation, we have augmented biases into the weight matrices, and the activation function is applied in component-wise manner. To simplify the notation we use Θ to denote all the model parameters $\Theta = \{\mathbf{W}_j\}_{j=1}^{M+1}$ in the FNN.

When the input and output dimensions are identical, i.e., $m = n$, residue network (ResNet) can be readily defined as

$$\mathbf{y}^{out} = [\mathbf{I}_m + \mathbf{N}(\cdot; \Theta)](\mathbf{y}^{in}), \quad (2.6)$$

where \mathbf{I}_m is the identity matrix of size $m \times m$. In this form, the neural network in fact models the difference between the input and output (thus the term ‘‘residue’’). Although mathematically equivalent to the original standard DNN, ResNet has been shown to be exceptionally useful in practice after its introduction in [14]. We will adopt the ResNet idea and modify it to our modeling work in the following section.

3. Main Method. In this section we present the main method for recovering (2.1). We first present our neural network approximation for the unknown equation in the context of flow map modeling. We then discuss its application for uncertainty quantification. Finally, we present analysis on the error estimation of our method.

3.1. Parameterized Flow Map. For given initial condition $\mathbf{x}_0 \in I_{\mathbf{x}}$ and parameter $\alpha \in I_{\alpha}$, the (unknown) dynamical system (2.1) defines a flow map

$$\mathbf{x}(s; \alpha, \mathbf{x}_0) = \Phi_{s-s_0}(\mathbf{x}(s_0; \alpha, \mathbf{x}_0), \alpha), \quad (3.1)$$

which maps the solution \mathbf{x} at time s_0 to the one at another different time s . Once again, only the time difference $s - s_0$ is relevant for autonomous systems considered in this paper. Consequently, for given time difference $\delta \in I_{\Delta}$, $\Phi_{\delta} : \mathbb{R}^d \times \mathbb{R}^l \rightarrow \mathbb{R}^d$ defines a map such that, for any parameter $\alpha \in I_{\alpha}$ and initial condition $\mathbf{x}_0 \in I_{\mathbf{x}}$,

$$\mathbf{x}(\delta; \alpha, \mathbf{x}_0) = \Phi_{\delta}(\mathbf{x}_0, \alpha). \quad (3.2)$$

For notational clarity, in the following we suppress the dependence on the initial condition \mathbf{x}_0 and use $\mathbf{x}(\delta; \alpha)$ in place of $\mathbf{x}(\delta; \alpha, \mathbf{x}_0)$.

Next, let us characterize the structure of the flow map more carefully. If we integrate the ODE (2.1) from 0 to δ , we have

$$\mathbf{x}(\delta; \alpha) = \mathbf{x}(0; \alpha) + \int_0^{\delta} \mathbf{f}(\mathbf{x}(s; \alpha), \alpha) ds = \mathbf{x}(0; \alpha) + \int_0^{\delta} \mathbf{f}(\Phi_s(\mathbf{x}(0; \alpha)), \alpha) ds. \quad (3.3)$$

We then have, for any fixed α and δ ,

$$\mathbf{x}(\delta; \alpha) = [\mathbf{I}_d + \Psi(\cdot, \alpha, \delta)](\mathbf{x}(0; \alpha)), \quad (3.4)$$

where \mathbf{I}_d is the identity matrix of size $d \times d$, and for any $\mathbf{z} \in I_{\mathbf{x}}$,

$$\Psi(\mathbf{z}, \alpha, \delta) = \int_0^{\delta} \mathbf{f}(\Phi_s(\mathbf{z}, \alpha), \alpha) ds \quad (3.5)$$

is the effective increment along a trajectory from \mathbf{z} over time lag δ . Upon comparing (3.4) with the ResNet operator (2.6), we see that ResNet provides a natural representation for flow map increment for fixed time lag δ and parameter α . We remark that this is an exact representation and without any approximation over the time horizon δ . Therefore, ResNet structure can be considered an exact time integrator in term of flow map ([26]).

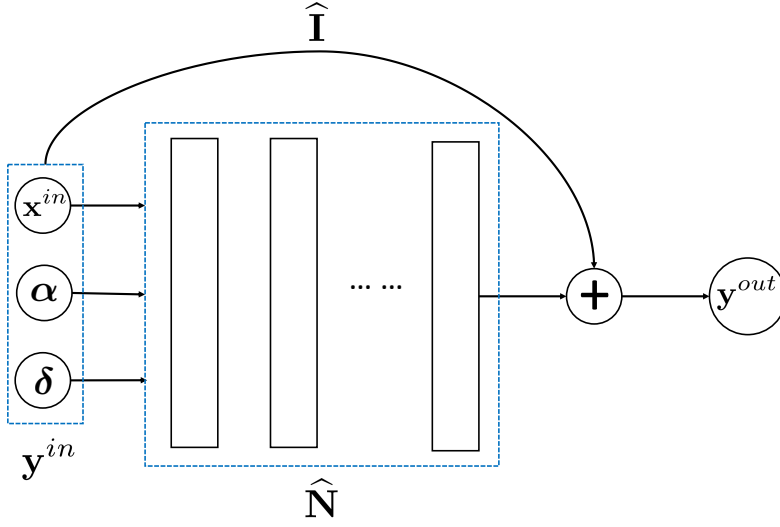


Fig. 3.1: Structure of the neural network.

3.2. Neural Network Model Construction. Straightforward application of ResNet, as proposed in [26], is only applicable for (3.4) for fixed α and δ . To model unknown system (2.1) with unknown parameters, we therefore propose a modified ResNet structure. The network structure is illustrated in Fig. 3.1. The input consists of the state variable \mathbf{x}^{in} , the parameters α and the time lag δ , i.e., $\mathbf{y}^{in} = [\mathbf{x}^{in}, \alpha, \delta]^\top$. Let us define a $(d + \ell + 1) \times (d + \ell + 1)$ matrix

$$\hat{\mathbf{I}} = \begin{bmatrix} \mathbf{I}_d & \mathbf{0} \\ \mathbf{0} & \mathbf{0} \end{bmatrix}, \quad (3.6)$$

where \mathbf{I}_d is the identity matrix of size $d \times d$. Then the network operator is defined as

$$\mathbf{y}^{out} = [\hat{\mathbf{I}} + \hat{\mathbf{N}}] (\mathbf{y}^{in}), \quad (3.7)$$

where $\hat{\mathbf{N}} : \mathbb{R}^{d+\ell+1} \rightarrow \mathbb{R}^d$ is the operator corresponding to the deep FNN. It is obvious that this is equivalent to

$$\mathbf{x}^{out}(\mathbf{x}^{in}, \alpha, \delta; \Theta) = \mathbf{x}^{in} + \hat{\mathbf{N}}(\mathbf{x}^{in}, \alpha, \delta; \Theta), \quad (3.8)$$

where Θ stands for the set of parameters in the neural network structure. By using the pair-wise data set (2.2), we set

$$\mathbf{z}_j^{(1)} \rightarrow (\mathbf{x}^{in}, \alpha, \delta), \quad \mathbf{z}_j^{(2)} \rightarrow \mathbf{x}^{out}.$$

The network training is conducted to find the neural network parameter set Θ^* that minimizes the mean-squared loss, i.e.,

$$\Theta^* = \underset{\Theta}{\operatorname{argmin}} \frac{1}{J} \sum_{j=1}^J \left\| \mathbf{x}^{out}(\mathbf{z}_j^{(1)}; \Theta) - \mathbf{z}_j^{(2)} \right\|^2, \quad (3.9)$$

Upon finding the optimal network parameter Θ^* , we obtain trained network model

$$\mathbf{x}(\delta; \boldsymbol{\alpha}) = \mathbf{x}(0; \boldsymbol{\alpha}) + \widehat{\mathbf{N}}(\mathbf{x}(0; \boldsymbol{\alpha}), \boldsymbol{\alpha}, \delta; \Theta^*), \quad \boldsymbol{\alpha} \in I_{\boldsymbol{\alpha}}, \quad \delta \in I_{\Delta}, \quad (3.10)$$

where I_{Δ} is the range of time lags in the dataset (2.2) and is defined in (2.4). Upon comparing to (3.4), it is obvious that the trained neural network $\widehat{\mathbf{N}}$ is an approximation to the parameterized effective increment $\boldsymbol{\Psi}$ in (3.5). That is,

$$\widehat{\mathbf{N}}(\mathbf{z}, \boldsymbol{\alpha}, \delta) \approx \boldsymbol{\Psi}(\mathbf{z}, \boldsymbol{\alpha}, \delta), \quad (\mathbf{z}, \boldsymbol{\alpha}, \delta) \in I_{\mathbf{x}} \times I_{\boldsymbol{\alpha}} \times I_{\Delta}. \quad (3.11)$$

The error in this approximation depends on the data quality and numerical training algorithm. Despite of this approximation error, the trained model (3.10) does not contain any error associated with time discretization. Therefore, the model (3.10) can be considered as an exact time integrator for the unknown parameterized system (2.1).

3.3. Prediction and Uncertainty Quantification. Once the model (3.10) is constructed, it serves as an approximation to the flow map of the original system (2.1). We can conduct system prediction via iterative use of the model. Let $\delta_k \in I_{\delta}$ be a sequence of time steps and \mathbf{x}_0 be a given initial condition. Then, for given system parameter $\boldsymbol{\alpha} \in I_{\boldsymbol{\alpha}}$, we have

$$\begin{cases} \widehat{\mathbf{x}}(t_0; \boldsymbol{\alpha}) = \mathbf{x}_0, \\ \widehat{\mathbf{x}}(t_{k+1}; \boldsymbol{\alpha}) = \widehat{\mathbf{x}}(t_k; \boldsymbol{\alpha}) + \widehat{\mathbf{N}}(\widehat{\mathbf{x}}(t_k; \boldsymbol{\alpha}), \boldsymbol{\alpha}, \delta_k; \Theta^*), \\ t_{k+1} = t_k + \delta_k, \quad k = 0, 1, \dots \end{cases} \quad (3.12)$$

These serve as approximation of the true solution $\mathbf{x}(t; \boldsymbol{\alpha}, \mathbf{x}_0)$ of the unknown system (2.1) at the time instances $t \in \{t_k, k = 0, 1, \dots\}$, with given parameter value $\boldsymbol{\alpha}$ and initial condition \mathbf{x}_0 .

When the system parameters $\boldsymbol{\alpha}$ are random, uncertainty quantification can be readily conducted by using the system prediction model (3.12). Let $\rho_{\boldsymbol{\alpha}}$ be the probability density the parameters $\boldsymbol{\alpha}$. Statistical information of the true solution $\mathbf{x}(t; \boldsymbol{\alpha})$ of (2.1) can approximated by applying the required statistical analysis on the approximate solution (3.12) generated by the network model (3.10), as a post-processing step. For example, the mean and variance of the solution can be approximated as

$$\begin{aligned} \mathbb{E}_{\boldsymbol{\alpha}}[\mathbf{x}(t; \boldsymbol{\alpha})] &\approx \mathbb{E}_{\boldsymbol{\alpha}}[\widehat{\mathbf{x}}(t; \boldsymbol{\alpha})] = \int_{I_{\boldsymbol{\alpha}}} \widehat{\mathbf{x}}(t; \mathbf{y}) \rho_{\boldsymbol{\alpha}}(\mathbf{y}) d\mathbf{y}, \\ \text{Var}_{\boldsymbol{\alpha}}[\mathbf{x}(t; \boldsymbol{\alpha})] &\approx \text{Var}_{\boldsymbol{\alpha}}[\widehat{\mathbf{x}}(t; \boldsymbol{\alpha})] = \int_{I_{\boldsymbol{\alpha}}} [\widehat{\mathbf{x}}(t; \mathbf{y}) - \mathbb{E}_{\boldsymbol{\alpha}}[\widehat{\mathbf{x}}(t; \mathbf{y})]]^2 \rho_{\boldsymbol{\alpha}}(\mathbf{y}) d\mathbf{y}. \end{aligned} \quad (3.13)$$

The integrals of $\widehat{\mathbf{x}}$ can be further approximated sampling based method, e.g., Monte Carlo or quadrature rule. This requires the predictive solution $\widehat{\mathbf{x}}$ at different sampling locations of $\boldsymbol{\alpha}$, which can be produced by the learned network model (3.12).

3.4. Theoretical properties. We now establish some theoretical analysis of the proposed methods. Our analysis relies on the celebrated universal approximation result for single hidden layer full connected feedforward neural network.

THEOREM 3.1. [25, Theorem 3.1] *For any given function $f \in C(\mathbb{R}^n)$ and positive real number $\epsilon > 0$, there exists a single-layer neural network $N(\cdot; \Theta)$ with parameter Θ such that*

$$\max_{\mathbf{x} \in D} |f(\mathbf{x}) - N(\mathbf{x}; \Theta)| < \epsilon$$

for any compact set $D \in \mathbb{R}^n$, if and only if the activation functions are continuous and are not polynomials.

Based on this result, we assume that the deep neural network used in our method can be trained such that the error in the approximation (3.11) can be sufficiently small. That is, for a given $\mathcal{E} > 0$

$$\left| \widehat{\mathbf{N}}(\mathbf{z}, \boldsymbol{\alpha}, \delta; \Theta^*) - \boldsymbol{\Psi}(\mathbf{z}, \boldsymbol{\alpha}, \delta) \right| \leq \mathcal{E}, \quad \forall (\mathbf{z}, \boldsymbol{\alpha}, \delta) \in I_{\mathbf{x}} \times I_{\boldsymbol{\alpha}} \times I_{\Delta}. \quad (3.14)$$

In the following, for any given n , set $t = \sum_{i=0}^{n-1} \delta_i$ as final time for the prediction, where $\delta_i \in I_{\Delta}$ as defined in (3.12).

LEMMA 3.2. *Suppose the right-hand-side $\mathbf{f}(\mathbf{x}, \boldsymbol{\alpha})$ of (2.1) is Lipschitz continuous with respect to \mathbf{x} with a uniform Lipschitz constant L , for all $\boldsymbol{\alpha} \in I_{\boldsymbol{\alpha}}$. If the trained neural network satisfies (3.14), then*

$$\|\widehat{\mathbf{x}}(t; \cdot, \cdot) - \mathbf{x}(t; \cdot, \cdot)\|_{L^\infty(I_{\boldsymbol{\alpha}} \times I_{\mathbf{x}})} \leq \frac{e^{nL\Delta} - 1}{e^{L\Delta} - 1} \mathcal{E}, \quad (3.15)$$

where $\mathbf{x}(t; \boldsymbol{\alpha}, \mathbf{x}_0)$ and $\widehat{\mathbf{x}}(t; \boldsymbol{\alpha}, \mathbf{x}_0)$ are as defined in (3.1) and (3.12), respectively.

Proof. First, for $(\mathbf{v}, \boldsymbol{\alpha}, \delta) \in I_{\mathbf{x}} \times I_{\boldsymbol{\alpha}} \times I_{\delta}$, by combining (3.2) and (3.4), we have

$$\boldsymbol{\Phi}_\delta(\mathbf{v}, \boldsymbol{\alpha}) = \mathbf{v} + \boldsymbol{\Psi}(\mathbf{v}, \boldsymbol{\alpha}, \delta).$$

Furthermore, (3.10) defines an approximated flow map

$$\widehat{\boldsymbol{\Phi}}_\delta(\mathbf{v}, \boldsymbol{\alpha}; \Theta^*) = \mathbf{v} + \widehat{\mathbf{N}}(\mathbf{v}, \boldsymbol{\alpha}, \delta; \Theta^*), \quad (\mathbf{v}, \boldsymbol{\alpha}, \delta) \in I_{\mathbf{x}} \times I_{\boldsymbol{\alpha}} \times I_{\delta}.$$

Next, for any $\mathbf{u}, \mathbf{v} \in I_{\mathbf{x}}$, and fixed $(\boldsymbol{\alpha}, \delta) \in I_{\boldsymbol{\alpha}} \times I_{\Delta}$, let us consider

$$\begin{aligned} \left| \boldsymbol{\Phi}_\delta(\mathbf{u}, \boldsymbol{\alpha}) - \widehat{\boldsymbol{\Phi}}_\delta(\mathbf{v}, \boldsymbol{\alpha}; \Theta^*) \right| &\leq \left| \boldsymbol{\Phi}_\delta(\mathbf{u}, \boldsymbol{\alpha}) - \boldsymbol{\Phi}_\delta(\mathbf{v}, \boldsymbol{\alpha}) \right| + \left| \boldsymbol{\Phi}_\delta(\mathbf{v}, \boldsymbol{\alpha}) - \widehat{\boldsymbol{\Phi}}_\delta(\mathbf{v}, \boldsymbol{\alpha}; \Theta^*) \right| \\ &= \left| \boldsymbol{\Phi}_\delta(\mathbf{u}, \boldsymbol{\alpha}) - \boldsymbol{\Phi}_\delta(\mathbf{v}, \boldsymbol{\alpha}) \right| + \left| \boldsymbol{\Psi}(\mathbf{v}, \boldsymbol{\alpha}, \delta) - \widehat{\mathbf{N}}(\mathbf{v}, \boldsymbol{\alpha}, \delta; \Theta^*) \right| \\ &\leq e^{L\Delta} |\mathbf{u} - \mathbf{v}| + \mathcal{E} \end{aligned} \quad (3.16)$$

where in the last step we have used (3.14) and the classical result on the continuity of dynamical system with respect to the initial data; see [38, p. 109].

Then for $t = \sum_{i=0}^{n-1} \delta_i$ with $\delta_i \in I_{\Delta}$, by (3.12), we have

$$\widehat{\mathbf{x}}(t; \mathbf{z}, \boldsymbol{\alpha}) = \widehat{\boldsymbol{\Phi}}_{\delta_{n-1}} \circ \widehat{\boldsymbol{\Phi}}_{\delta_{n-2}} \circ \cdots \circ \widehat{\boldsymbol{\Phi}}_{\delta_0}(\mathbf{z}, \boldsymbol{\alpha}; \Theta^*).$$

Moreover, by the time invariance of autonomous system, we have

$$\mathbf{x}(t; \mathbf{z}, \boldsymbol{\alpha}) = \boldsymbol{\Phi}_{\delta_{n-1}} \circ \boldsymbol{\Phi}_{\delta_{n-2}} \circ \cdots \circ \boldsymbol{\Phi}_{\delta_0}(\mathbf{z}, \boldsymbol{\alpha}).$$

Then, by repeatedly employing (3.16), we have

$$\begin{aligned}
& |\widehat{\mathbf{x}}(t; \mathbf{z}, \boldsymbol{\alpha}) - \mathbf{x}(t; \mathbf{z}, \boldsymbol{\alpha})| \\
&= \left| \widehat{\Phi}_{\delta_{n-1}} \circ \widehat{\Phi}_{\delta_{n-2}} \circ \cdots \circ \widehat{\Phi}_{\delta_0}(\mathbf{z}, \boldsymbol{\alpha}; \Theta^*) - \Phi_{\delta_{n-1}} \circ \Phi_{\delta_{n-2}} \circ \cdots \circ \Phi_{\delta_0}(\mathbf{z}; \boldsymbol{\alpha}) \right| \\
&\leq \mathcal{E} + e^{L\delta_{n-1}} \left| \widehat{\Phi}_{\delta_{n-2}} \circ \cdots \circ \widehat{\Phi}_{\delta_0}(\mathbf{z}, \boldsymbol{\alpha}; \Theta^*) - \Phi_{\delta_{n-2}} \circ \cdots \circ \Phi_{\delta_0}(\mathbf{z}; \boldsymbol{\alpha}) \right| \\
&\leq \mathcal{E} + e^{L\delta_{n-1}} \left[\mathcal{E} + e^{L\delta_{n-2}} \left| \widehat{\Phi}_{\delta_{n-3}} \circ \cdots \circ \widehat{\Phi}_{\delta_0}(\mathbf{z}, \boldsymbol{\alpha}; \Theta^*) - \Phi_{\delta_{n-3}} \circ \cdots \circ \Phi_{\delta_0}(\mathbf{z}; \boldsymbol{\alpha}) \right| \right] \\
&\leq \dots \\
&\leq \mathcal{E} \left(1 + e^{L\delta_{n-1}} + e^{L(\delta_{n-1} + \delta_{n-2})} + \dots + e^{L\sum_{i=1}^{n-1} \delta_i} \right) \\
&\leq \mathcal{E} \left(1 + e^{L\Delta} + e^{2L\Delta} + \dots + e^{(n-1)L\Delta} \right) \\
&= \frac{e^{nL\Delta} - 1}{e^{L\Delta} - 1} \mathcal{E}
\end{aligned}$$

for any $(\boldsymbol{\alpha}, \mathbf{z}) \in I_{\boldsymbol{\alpha}} \times I_{\mathbf{x}}$. This implies the result (3.15). \square

When the trained network is used for UQ as in (3.13), we obtain the following estimates.

THEOREM 3.3. *Under the same assumptions of Lemma 3.2 and assume for a fixed initial condition \mathbf{x}_0 , the solution is bounded $\|\mathbf{x}(t; \cdot)\|_{L^\infty(I_{\boldsymbol{\alpha}})} = C_t < \infty$. Then,*

$$|\mathbb{E}_{\boldsymbol{\alpha}}[\mathbf{x}(t; \boldsymbol{\alpha})] - \mathbb{E}_{\boldsymbol{\alpha}}[\widehat{\mathbf{x}}(t; \boldsymbol{\alpha})]| \leq C(n, L, \Delta)\mathcal{E}, \quad (3.17)$$

$$|\text{Var}_{\boldsymbol{\alpha}}[\mathbf{x}(t; \boldsymbol{\alpha})] - \text{Var}_{\boldsymbol{\alpha}}[\widehat{\mathbf{x}}(t; \boldsymbol{\alpha})]| \leq 2C(n, L, \Delta)^2 \mathcal{E}^2 + 4C(n, L, \Delta)C_t \mathcal{E}, \quad (3.18)$$

where $C(n, L, \Delta) = \frac{e^{nL\Delta} - 1}{e^{L\Delta} - 1}$.

Proof. For the mean approximation (3.17), by Lemma 3.2, we have

$$|\mathbb{E}_{\boldsymbol{\alpha}}[\mathbf{x}(t; \boldsymbol{\alpha})] - \mathbb{E}_{\boldsymbol{\alpha}}[\widehat{\mathbf{x}}(t; \boldsymbol{\alpha})]| \leq \mathbb{E}_{\boldsymbol{\alpha}}[|\mathbf{x}(t; \boldsymbol{\alpha}) - \widehat{\mathbf{x}}(t; \boldsymbol{\alpha})|] \leq \frac{e^{nL\Delta} - 1}{e^{L\Delta} - 1} \mathcal{E}.$$

For the variance approximation, we have

$$\begin{aligned}
& |\text{Var}_{\boldsymbol{\alpha}}[\mathbf{x}(t; \boldsymbol{\alpha})] - \text{Var}_{\boldsymbol{\alpha}}[\widehat{\mathbf{x}}(t; \boldsymbol{\alpha})]| \\
&= |\mathbb{E}_{\boldsymbol{\alpha}}[\mathbf{x}(t; \boldsymbol{\alpha})^2] - \mathbb{E}_{\boldsymbol{\alpha}}[\mathbf{x}(t; \boldsymbol{\alpha})]^2 - \mathbb{E}_{\boldsymbol{\alpha}}[\widehat{\mathbf{x}}(t; \boldsymbol{\alpha})^2] + \mathbb{E}_{\boldsymbol{\alpha}}[\widehat{\mathbf{x}}(t; \boldsymbol{\alpha})]^2| \\
&\leq |\mathbb{E}_{\boldsymbol{\alpha}}[\mathbf{x}(t; \boldsymbol{\alpha})^2] - \mathbb{E}_{\boldsymbol{\alpha}}[\widehat{\mathbf{x}}(t; \boldsymbol{\alpha})^2]| + |\mathbb{E}_{\boldsymbol{\alpha}}[\mathbf{x}(t; \boldsymbol{\alpha})]^2 - \mathbb{E}_{\boldsymbol{\alpha}}[\widehat{\mathbf{x}}(t; \boldsymbol{\alpha})]^2| \\
&= \mathbb{E}_{\boldsymbol{\alpha}}[|\mathbf{x}(t; \boldsymbol{\alpha}) - \widehat{\mathbf{x}}(t; \boldsymbol{\alpha})| |\mathbf{x}(t; \boldsymbol{\alpha}) + \widehat{\mathbf{x}}(t; \boldsymbol{\alpha})|] \\
&\quad + \mathbb{E}_{\boldsymbol{\alpha}}[|\mathbf{x}(t; \boldsymbol{\alpha}) - \widehat{\mathbf{x}}(t; \boldsymbol{\alpha})|] \mathbb{E}_{\boldsymbol{\alpha}}[|\mathbf{x}(t; \boldsymbol{\alpha}) + \widehat{\mathbf{x}}(t; \boldsymbol{\alpha})|] \\
&\leq 2 \frac{(e^{nL\Delta} - 1)\mathcal{E}}{e^{L\Delta} - 1} \mathbb{E}_{\boldsymbol{\alpha}}[|\mathbf{x}(t; \boldsymbol{\alpha}) + \widehat{\mathbf{x}}(t; \boldsymbol{\alpha})|] \\
&\leq 2 \frac{(e^{nL\Delta} - 1)\mathcal{E}}{e^{L\Delta} - 1} (\mathbb{E}_{\boldsymbol{\alpha}}[|\widehat{\mathbf{x}}(t; \boldsymbol{\alpha}) - \mathbf{x}(t; \boldsymbol{\alpha})|] + \mathbb{E}_{\boldsymbol{\alpha}}[|2\mathbf{x}(t; \boldsymbol{\alpha})|]) \\
&\leq 2 \frac{(e^{nL\Delta} - 1)^2}{(e^{L\Delta} - 1)^2} \mathcal{E}^2 + 4 \frac{(e^{nL\Delta} - 1)C_t}{e^{L\Delta} - 1} \mathcal{E}
\end{aligned}$$

This gives the result (3.18). \square

In practice, the true parameter range $I_{\boldsymbol{\alpha}}$ is sometimes unknown, due to our lack of knowledge of the underlying physical system and is usually replaced by an estimated range $\widetilde{I}_{\boldsymbol{\alpha}}$, in which the ODE (2.1) is assumed to be well-posed. Suppose the

distribution of parameters on the estimated range \tilde{I}_α is $\tilde{\rho}_\alpha$. Then, as in [16, 5], the mean and variance can be approximated by

$$\begin{aligned}\mathbb{E}_\alpha[\mathbf{x}(t; \boldsymbol{\alpha})] &\approx \tilde{\mathbb{E}}_\alpha[\hat{\mathbf{x}}(t; \boldsymbol{\alpha})] = \int_{\tilde{I}_\alpha} \hat{\mathbf{x}}(t; \mathbf{y}) \tilde{\rho}_\alpha(\mathbf{y}) d\mathbf{y}, \\ \text{Var}_\alpha[\mathbf{x}(t; \boldsymbol{\alpha})] &\approx \widetilde{\text{Var}}_\alpha[\hat{\mathbf{x}}(t; \boldsymbol{\alpha})] = \int_{\tilde{I}_\alpha} \left[\hat{\mathbf{x}}(t; \mathbf{y}) - \tilde{E}_\alpha[\hat{\mathbf{x}}(t; \mathbf{y})] \right]^2 \tilde{\rho}_\alpha(\mathbf{y}) d\mathbf{y}.\end{aligned}\quad (3.19)$$

Let us define

$$I_\alpha^o = I_\alpha \cap \tilde{I}_\alpha, \quad I_\alpha^- = I_\alpha / I_\alpha^o, \quad \tilde{I}_\alpha^- = \tilde{I}_\alpha / I_\alpha^o.$$

Suppose

$$\int_{I_\alpha^o} |\rho_\alpha(\mathbf{y}) - \tilde{\rho}_\alpha(\mathbf{y})| d\mathbf{y} \leq \gamma \quad (3.20)$$

and the difference between I_α and \tilde{I}_α is small in the sense that

$$\int_{\tilde{I}_\alpha^-} \tilde{\rho}_\alpha(\mathbf{y}) d\mathbf{y} + \int_{I_\alpha^-} \rho_\alpha(\mathbf{y}) d\mathbf{y} \leq \eta \quad (3.21)$$

for some small positive number γ and η , then we have the following results concerning the error in the approximation (3.19).

THEOREM 3.4. *Under the assumptions in Lemma 3.2 and assume the distribution $\tilde{\rho}_\alpha$ and the estimated parameter range \tilde{I}_α satisfy (3.20) and (3.21). In addition, assume that $\|\mathbf{x}(t; \cdot)\|_{L^\infty(\tilde{I}_\alpha \cup I_\alpha)} \leq \tilde{C}_t$, then we have*

$$\left| \mathbb{E}_\alpha[\mathbf{x}(t; \boldsymbol{\alpha})] - \tilde{\mathbb{E}}_\alpha[\hat{\mathbf{x}}(t; \boldsymbol{\alpha})] \right| \leq \tilde{C}_t(\eta + \gamma) + C(1 + \eta)\mathcal{E}, \quad (3.22)$$

$$\begin{aligned}\left| \text{Var}_\alpha[\mathbf{x}(t; \boldsymbol{\alpha})] - \widetilde{\text{Var}}_\alpha[\hat{\mathbf{x}}(t; \boldsymbol{\alpha})] \right| &\leq (3\tilde{C}_t^2 + C\tilde{C}_t\mathcal{E})(\eta + \gamma) \\ &\quad + (4\tilde{C}_t + 2C\mathcal{E})(1 + \eta)C\mathcal{E},\end{aligned}\quad (3.23)$$

where $C = \frac{e^{nL\Delta} - 1}{e^{L\Delta} - 1}$.

Proof. First, let us show the error estimate for the approximation of the expect-

tation in (3.22). To this end, we have the following sequence of estimates.

$$\begin{aligned}
& \left| \mathbb{E}_\alpha[\mathbf{x}(t; \boldsymbol{\alpha})] - \widetilde{\mathbb{E}}_\alpha[\widehat{\mathbf{x}}(t; \boldsymbol{\alpha})] \right| \\
&= \left| \int_{I_\alpha} \mathbf{x}(t; \mathbf{y}) \rho_\alpha(\mathbf{y}) d\mathbf{y} - \int_{\widetilde{I}_\alpha} \widehat{\mathbf{x}}(t; \mathbf{y}) \widetilde{\rho}_\alpha(\mathbf{y}) d\mathbf{y} \right| \\
&= \left| \int_{I_\alpha^-} \mathbf{x}(t; \mathbf{y}) \rho_\alpha(\mathbf{y}) d\mathbf{y} + \int_{I_\alpha^0} \mathbf{x}(t; \mathbf{y}) \rho_\alpha(\mathbf{y}) d\mathbf{y} - \int_{\widetilde{I}_\alpha^-} \widehat{\mathbf{x}}(t; \mathbf{y}) \widetilde{\rho}_\alpha(\mathbf{y}) d\mathbf{y} - \int_{I_\alpha^0} \widehat{\mathbf{x}}(t; \mathbf{y}) \widetilde{\rho}_\alpha(\mathbf{y}) d\mathbf{y} \right| \\
&\leq \int_{I_\alpha^-} |\mathbf{x}(t; \mathbf{y})| \rho_\alpha(\mathbf{y}) d\mathbf{y} + \int_{\widetilde{I}_\alpha^-} |\widehat{\mathbf{x}}(t; \mathbf{y})| \widetilde{\rho}_\alpha(\mathbf{y}) d\mathbf{y} + \\
&\quad \left| \int_{I_\alpha^0} \mathbf{x}(t; \mathbf{y}) (\rho_\alpha(\mathbf{y}) - \widetilde{\rho}_\alpha(\mathbf{y})) d\mathbf{y} + \int_{I_\alpha^0} (\mathbf{x}(t; \mathbf{y}) - \widehat{\mathbf{x}}(t; \mathbf{y})) \widetilde{\rho}_\alpha(\mathbf{y}) d\mathbf{y} \right| \\
&\leq \|\mathbf{x}(t; \cdot)\|_{L^\infty} \int_{I_\alpha^-} \rho_\alpha(\mathbf{y}) d\mathbf{y} + \|\widehat{\mathbf{x}}(t; \cdot)\|_{L^\infty} \int_{\widetilde{I}_\alpha^-} \widetilde{\rho}_\alpha(\mathbf{y}) d\mathbf{y} + \int_{I_\alpha^0} |\mathbf{x}(t; \mathbf{y})| |\rho_\alpha(\mathbf{y}) - \widetilde{\rho}_\alpha(\mathbf{y})| d\mathbf{y} \\
&\quad + \int_{I_\alpha^0} |\mathbf{x}(t; \mathbf{y}) - \widehat{\mathbf{x}}(t; \mathbf{y})| \widetilde{\rho}_\alpha(\mathbf{y}) d\mathbf{y} \\
&\leq \|\mathbf{x}(t; \cdot)\|_{L^\infty} \int_{I_\alpha^-} \rho_\alpha(\mathbf{y}) d\mathbf{y} + (\|\mathbf{x}(t; \cdot)\|_{L^\infty} + \|\mathbf{x}(t; \cdot) - \widehat{\mathbf{x}}(t; \cdot)\|_{L^\infty}) \int_{\widetilde{I}_\alpha^-} \widetilde{\rho}_\alpha(\mathbf{y}) d\mathbf{y} \\
&\quad + \|\mathbf{x}(t; \cdot)\|_{L^\infty} \int_{I_\alpha^0} |\rho_\alpha(\mathbf{y}) - \widetilde{\rho}_\alpha(\mathbf{y})| d\mathbf{y} + \|\mathbf{x}(t; \cdot) - \widehat{\mathbf{x}}(t; \cdot)\|_{L^\infty} \int_{I_\alpha^0} \widetilde{\rho}_\alpha(\mathbf{y}) d\mathbf{y} \\
&\leq [\widetilde{C}_t + C\mathcal{E}] \eta + \widetilde{C}_t \gamma + C\mathcal{E} \\
&= \widetilde{C}_t(\eta + \gamma) + C(1 + \eta)\mathcal{E}
\end{aligned}$$

which establishes the result (3.22). In the last step, we have used (3.15), (3.20), and (3.21).

Next, we consider the approximation of the variance. By the definition of the variance approximation in (3.23), we have

$$\begin{aligned}
& \left| \text{Var}_\alpha[\mathbf{x}(t; \boldsymbol{\alpha})] - \widetilde{\text{Var}}_\alpha[\widehat{\mathbf{x}}(t; \boldsymbol{\alpha})] \right| \\
&= \left| \mathbb{E}_\alpha[\mathbf{x}(t; \boldsymbol{\alpha})^2] - \mathbb{E}_\alpha[\mathbf{x}(t; \boldsymbol{\alpha})]^2 - \widetilde{\mathbb{E}}_\alpha[\mathbf{x}(t; \boldsymbol{\alpha})^2] + \widetilde{\mathbb{E}}_\alpha[\mathbf{x}(t; \boldsymbol{\alpha})]^2 \right| \\
&\leq \left| \mathbb{E}_\alpha[\mathbf{x}(t; \boldsymbol{\alpha})^2] - \widetilde{\mathbb{E}}_\alpha[\mathbf{x}(t; \boldsymbol{\alpha})^2] \right| + \left| \mathbb{E}_\alpha[\mathbf{x}(t; \boldsymbol{\alpha})]^2 - \widetilde{\mathbb{E}}_\alpha[\mathbf{x}(t; \boldsymbol{\alpha})]^2 \right|
\end{aligned}$$

For the first term, since $\|\mathbf{x}(t; \cdot)^2\|_{L^\infty(I_\alpha \cup \widetilde{I}_\alpha)} \leq \widetilde{C}_t^2$ and

$$\begin{aligned}
\|\mathbf{x}(t; \cdot)^2 - \widehat{\mathbf{x}}(t; \cdot)^2\|_{L^\infty(I_\alpha \times \widetilde{I}_\alpha)} &\leq \|\mathbf{x}(t; \cdot) - \widehat{\mathbf{x}}(t; \cdot)\|_{L^\infty(\widetilde{I}_\alpha)} \|\mathbf{x}(t; \cdot) + \widehat{\mathbf{x}}(t; \cdot)\|_{L^\infty(\widetilde{I}_\alpha)} \\
&\leq C\mathcal{E} \left(C\mathcal{E} + 2\widetilde{C}_t \right),
\end{aligned}$$

by the proof for (3.22) we have

$$\left| \mathbb{E}_\alpha[\mathbf{x}(t; \boldsymbol{\alpha})^2] - \widetilde{\mathbb{E}}_\alpha[\mathbf{x}(t; \boldsymbol{\alpha})^2] \right| \leq \widetilde{C}_t^2(\eta + \gamma) + (1 + \eta)(2\widetilde{C}_t C\mathcal{E} + C^2\mathcal{E}^2). \quad (3.24)$$

For the second term, since

$$\left| \mathbb{E}_\alpha[\mathbf{x}(t; \boldsymbol{\alpha})] \right| \leq \widetilde{C}_t, \quad \left| \widetilde{\mathbb{E}}_\alpha[\widehat{\mathbf{x}}(t; \boldsymbol{\alpha})] \right| \leq (\widetilde{C}_t + C\mathcal{E}),$$

we have

$$\begin{aligned}
& \left| \mathbb{E}_\alpha[\mathbf{x}(t; \boldsymbol{\alpha})]^2 - \widetilde{\mathbb{E}}_\alpha[\mathbf{x}(t; \boldsymbol{\alpha})]^2 \right| \\
& \leq \left| \mathbb{E}_\alpha[\mathbf{x}(t; \boldsymbol{\alpha})] - \widetilde{\mathbb{E}}_\alpha[\mathbf{x}(t; \boldsymbol{\alpha})] \right| \left| \mathbb{E}_\alpha[\mathbf{x}(t; \boldsymbol{\alpha})] + \widetilde{\mathbb{E}}_\alpha[\mathbf{x}(t; \boldsymbol{\alpha})] \right| \\
& \leq \left[\widetilde{C}_t(\eta + \gamma) + C(1 + \eta)\mathcal{E} \right] (2\widetilde{C}_t + C\mathcal{E}). \tag{3.25}
\end{aligned}$$

By combining (3.24) and (3.25), we have

$$\begin{aligned}
\left| \text{Var}_\alpha[\mathbf{x}(t; \boldsymbol{\alpha})] - \widetilde{\text{Var}}_\alpha[\widehat{\mathbf{x}}(t; \boldsymbol{\alpha})] \right| & \leq (3\widetilde{C}_t^2 + C\widetilde{C}_t\mathcal{E})(\eta + \gamma) \\
& \quad + (4\widetilde{C}_t + 2C\mathcal{E})(1 + \eta)C\mathcal{E}.
\end{aligned}$$

This complete the proof for (3.23). \square

4. Numerical Examples. In this section we present numerical examples to verify the performance and properties of the proposed methods. For benchmarking purpose, we utilize examples with known governing parameterized equations. We use the true equations only to generate synthetic data. Once the neural network models are constructed using the data, we conduct predictions using the trained model and compare them against the high resolution numerical solutions of the true equations. In all the examples, time lags, initial states and parameters are sampled uniformly from $I_\Delta \times I_{\mathbf{x}} \times I_\alpha$. While we set $I_\Delta = [0, \Delta]$ with $\Delta = 0.1$ for all examples, the state variable domain $I_{\mathbf{x}}$ and the parameter domain I_α vary and are specified in each example.

We use (M, n) to denote the structure of $\widehat{\mathbf{N}}$, where M denotes the number of hidden layers and n denotes the number of nodes in each layer. The activation function is chosen as $\sigma = \tanh(x)$ (no noticeable difference were observed when using other activation functions such as ReLU). We generate data training set by randomly sampling $20m$ data pairs, where m is the number of parameters in the network model. The DNNs are trained by minimizing the mean square loss function in (3.9) by using the Adam algorithm [18] with the standard parameters with the open-source Tensorflow library [1]. The training data set is divided into mini-batches of size 30. And we typically train the model for 2,000 epochs and reshuffle the training data in each epoch. All the weights are initialized randomly from Gaussian distributions and all the biases are initialized to be zeros.

4.1. Example 1: Linear Scalar ODE. Let us first consider the following linear ODE with a single random parameter

$$\frac{dx}{dt} = -\alpha x, \quad x(0) = x_0, \tag{4.1}$$

where α is a random coefficient. We take $I_\alpha = [0, 1]$ and $I_x = [0, 1]$. This simple parameterized equation has the following analytical solution

$$x(t; \alpha, x_0) = x_0 e^{-\alpha t}.$$

We approximate the flow map with DNN of structure (3, 40). We first test the l^∞ and l^2 error of 100 sample trajectories. The trained network with a given sample parameter is composed for 300 times and makes predictions till $t = 30$. The error plots are shown in Fig. 4.1. We observe that the error grows with time, which is as

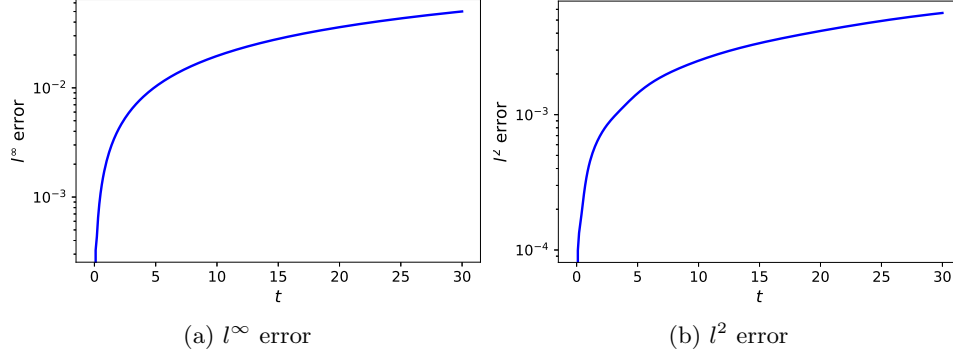


Fig. 4.1: The l^∞ (left) and l^2 (right) error of sample trajectories for Example 1 with $x_0 = 1$.

expected by Lemma 3.2, and stays around 10^{-2} . If α is uniformly distributed in the interval $[0, 1]$, the exact mean of the solution is

$$\mathbb{E}_\alpha[x(t; \alpha)] = \int_0^1 e^{-\alpha t} d\alpha = \frac{1 - e^{-t}}{t},$$

and the variance is

$$\text{Var}_\alpha[x(t; \alpha)] = \frac{1 - e^{-2t}}{2t} - \left(\frac{1 - e^{-t}}{t} \right)^2. \quad (4.2)$$

The approximate mean and variance of the DNN approximation of the governing equations are computed by applying a ten-point Gauss-Legendre quadrature over the parameter interval I_α to approximate the integrals in (3.13). In Fig. 4.2, we show the approximate mean and variance of sample trajectories. The results are comparable with the results obtained by the time-dependent gPC in [9]. In Fig. 4.1, we also

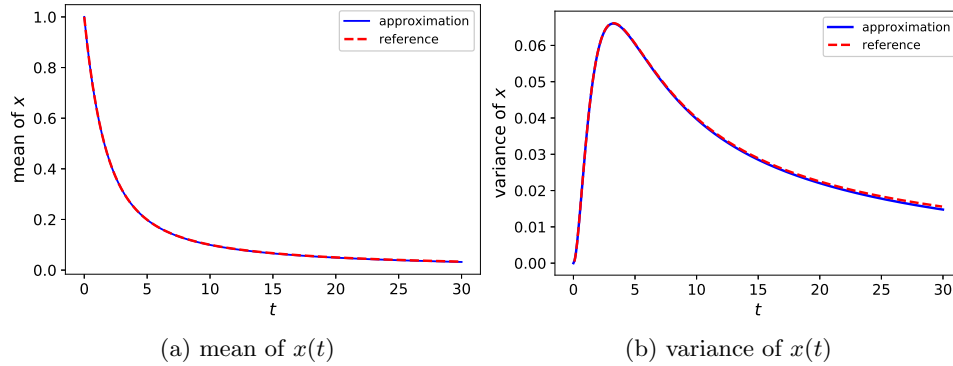


Fig. 4.2: Mean and variance of the solution to Example 1 with $x_0 = 1$.

present the propagation of errors in the mean and variance. We observe that the

errors in mean solution grow first and then stays at a level of around 10^{-3} after 150 steps of compositions. The errors in variance continue to grow exponentially with n , as expected by the error estimate in (3.18).

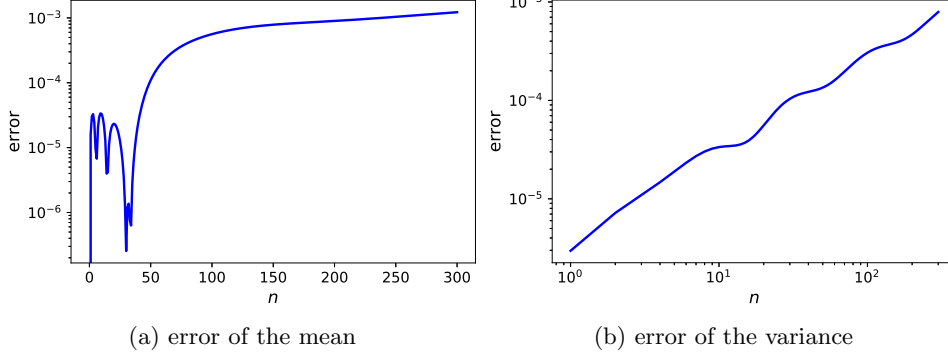


Fig. 4.3: The propagation of errors in mean (left) and variance (right) of the solution to Example 1 with $x_0 = 1$.

4.2. Example 2: Linear ODE System. We now consider a linear ODE system

$$\begin{aligned} \frac{dx_1}{dt} &= x_1 - \alpha_1 x_2, \\ \frac{dx_2}{dt} &= \alpha_2 x_1 - 7x_2, \end{aligned} \tag{4.3}$$

with $\alpha = (\alpha_1, \alpha_2) \in I_\alpha = (3.8, 4.2)^2$ and $I_x = [-1, 1]^2$. We use a fully connected block of the structure (3, 40) to construct the DNN model (3.10). After the training of the DNN is complete, we randomly draw 1,000 sample parameters uniformly from I_α and estimate the associated trajectories for $t \in [0, 10]$ and starting from $\mathbf{x}_0 = (0, 1)$. The l^∞ and l^2 errors for these trajectories are shown in Fig. 4.4.

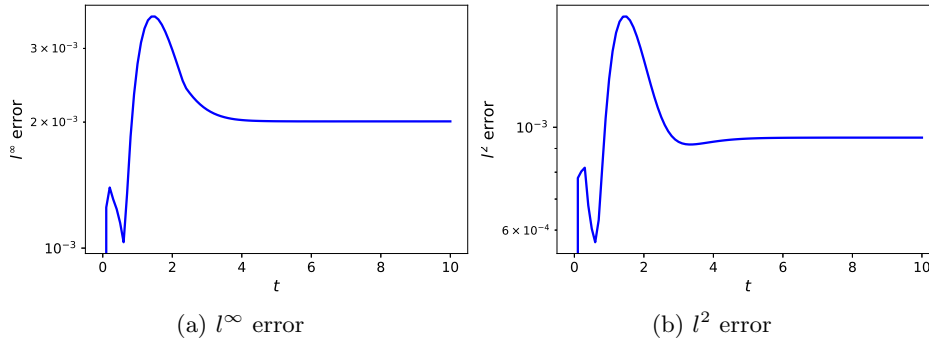


Fig. 4.4: The l^∞ (left) and l^2 (right) error of sample trajectories for Example 2 with $\mathbf{x}_0 = (0, 1)$.

For UQ, we set the parameters α to follow a multivariate uniform distribution over I_α . In Fig. 4.5, the approximated mean and variance, computed using a tensor product of five-point Gauss-Legendre quadrature, are presented. Good match between the DNN approximation and the reference is observed. In Fig. 4.6, we see that the error in the mean and the variance is around 10^{-3} and 10^{-5} , respectively.

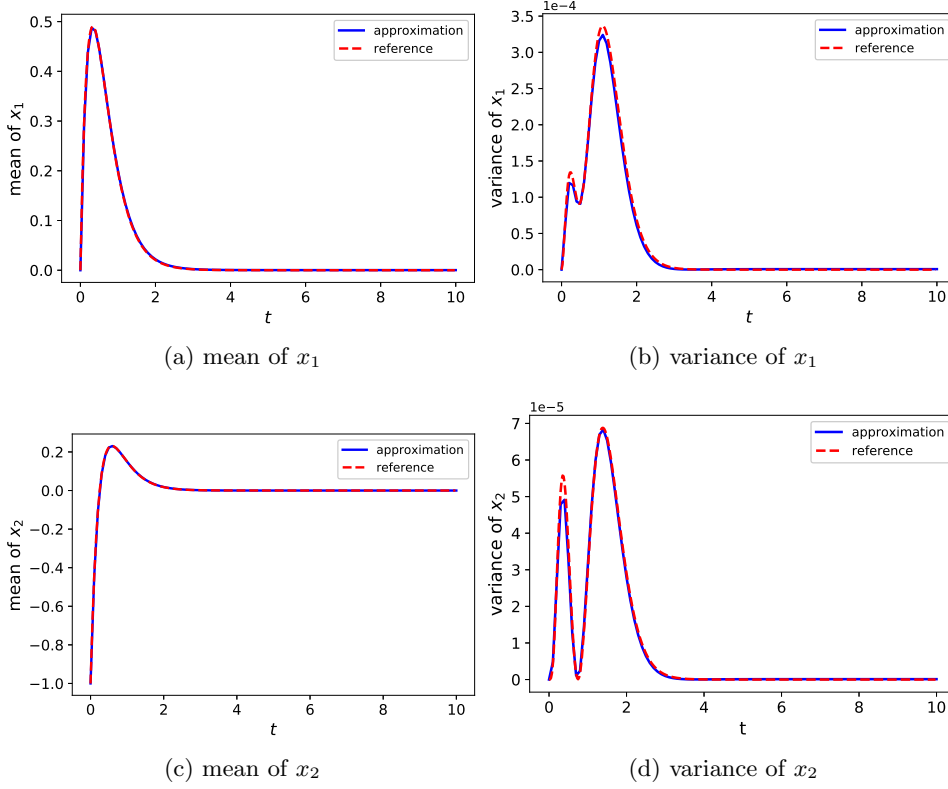


Fig. 4.5: Mean and variance of the solution to Example 2 with $\mathbf{x}_0 = (0, -1)$.

4.3. Example 3: Nonlinear Random Oscillation. We now consider a nonlinear system of ODEs,

$$\begin{aligned} \frac{dx_1}{dt} &= x_2, \\ \frac{dx_2}{dt} &= -\alpha_1 x_2 - \alpha_2 \sin x_1, \end{aligned} \tag{4.4}$$

where $\alpha = (\alpha_1, \alpha_2) \in I_\alpha = [0, 0.4] \times [8.8, 9.2]$ and $I_x = [-\pi, \pi] \times [-2\pi, 2\pi]$.

The flow map is approximated by a DNN with structure (3, 40). The l^∞ and l^2 errors for 1000 sample trajectories with $\mathbf{x}_0 = (-1.193, -3.876)$ and $t = 20$ are presented in Fig. 4.7. The error grows with time and stay around 10^{-2} . The oscillation is due the oscillatory behavior of the solution.

The mean and variance are computed in the same way as in Example 2. We present the results in Fig. 4.8. A good performance is observed for the approximation

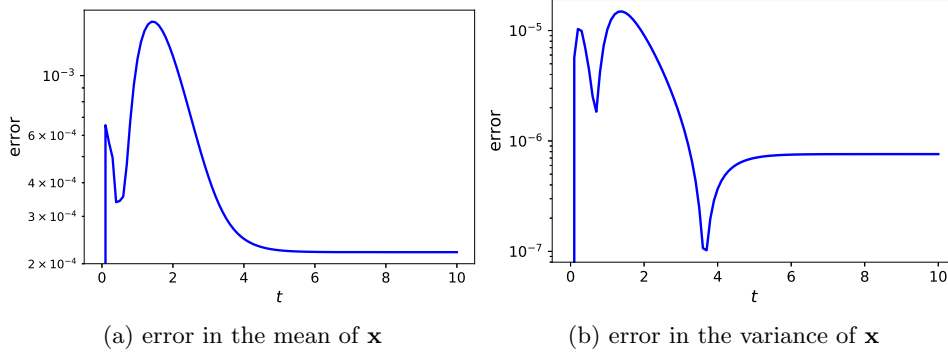


Fig. 4.6: The error of the mean and variance for Example 2.

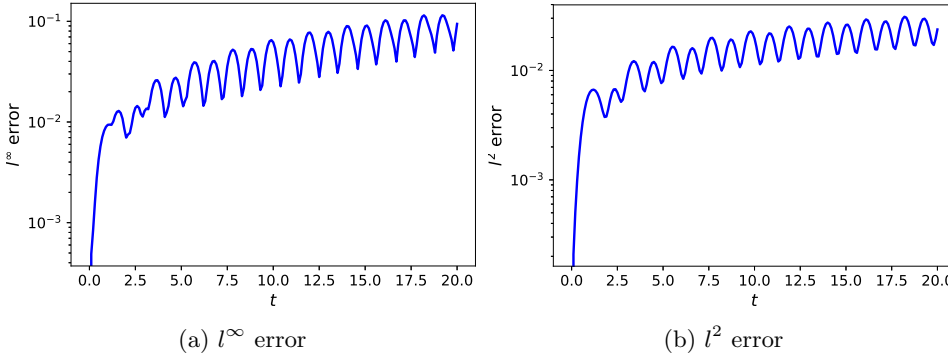


Fig. 4.7: The l^∞ (left) and l^2 (right) errors of sample trajectories of Example 3 with $\mathbf{x}_0 = (-1.193, -3.876)$.

for both the mean and the variance. For the variance approximation, a slight deviation is observed after $t = 12.5$, i.e., $n = 125$. This is due to the accumulation of the error as shown in (3.18). We further plot the propagation of the error of the variance approximation in Fig. 4.7. The error grows slowly and oscillates with respect to t .

4.4. Example 4: Cell Signaling Cascade. The last example is nonlinear system with moderately high dimensional parameter inputs. It is a mathematical model for autocrine cell-signaling loop developed in [36] in the following form

$$\begin{aligned}
 \frac{de_{1p}}{dt} &= \frac{I}{1 + Ge_{3p}} \frac{V_{\max,1}(1 - e_{1p})}{K_{m,1} + (1 - e_{1p})} - \frac{V_{\max,2}e_{1p}}{K_{m,2} + e_{1p}}, \\
 \frac{de_{2p}}{dt} &= \frac{V_{\max,3}e_{1p}(1 - e_{2p})}{K_{m,3} + (1 - e_{2p})} - \frac{V_{\max,4}e_{2p}}{K_{m,4} + e_{2p}}, \\
 \frac{de_{3p}}{dt} &= \frac{V_{\max,5}e_{2p}(1 - e_{3p})}{K_{m,5} + (1 - e_{3p})} - \frac{V_{\max,6}e_{3p}}{K_{m,6} + e_{3p}}.
 \end{aligned} \tag{4.5}$$

The state variables e_{1p} , e_{2p} , and e_{3p} denote the dimensionless concentrations of the active form of the enzymes. This model contains 13 (random) parameters: $K_{m,1-6}$,

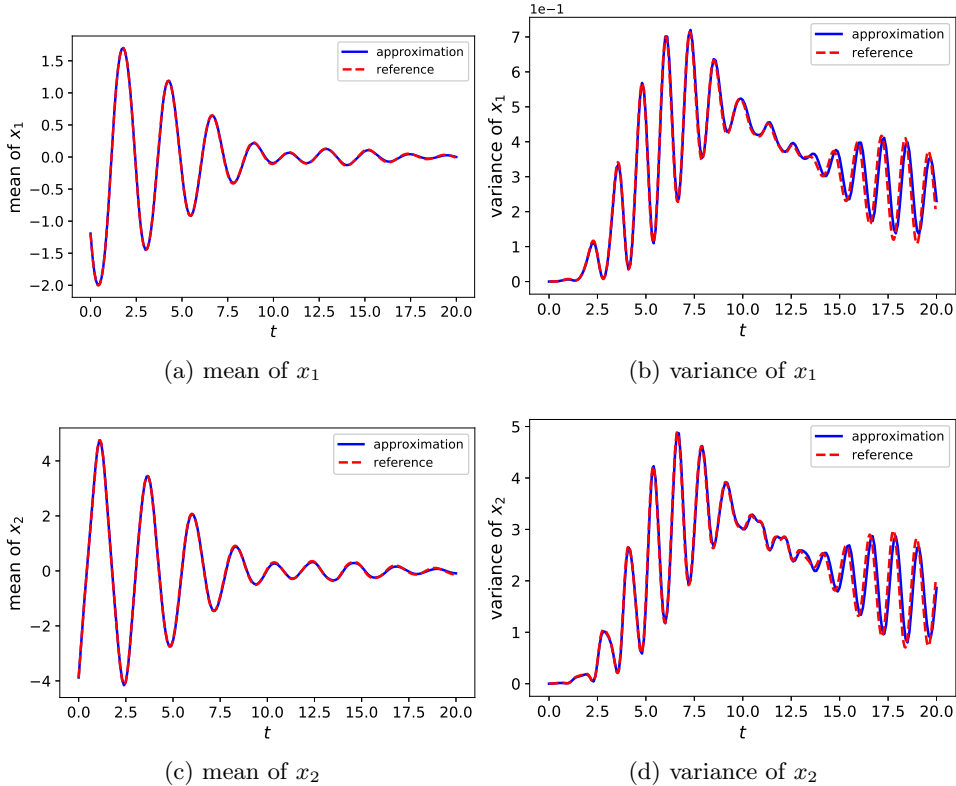


Fig. 4.8: Mean (left column) and variance (right column) of the solution to Example 3 with $\mathbf{x}_0 = (-1.193, -3.876)$.

$V_{\max,1-6}$, and G , and a tuning parameter I with range $[0, 1.5]$. In [36], the parameters take the following values $K_{m,1-6} = 0.2$, $V_{\max,1} = 0.5$, $V_{\max,2} = 0.15$, $V_{\max,3} = 0.15$, $V_{\max,4} = 0.15$, $V_{\max,5} = 0.25$, $V_{\max,6} = 0.05$, and $G = 2$. Here, we use these values as the mean values for the parameters and assume all parameters are independently and uniformly distributed in a hypercube of $\pm 10\%$ around the mean values.

Each concentration should fall between 0 and 1 and hence we take $I_{\mathbf{x}} = [0, 1]^3$. Moreover, to ensure the output of the DNN falls in this physical bound, we add an activation function $\sigma_{\text{output}} = \tanh(x)$ on each output node. The fully connected block in the network employed here has a structure with 3 layers and 200 nodes each layer. For illustration purpose, we calculate the mean and variance of the state variables with respect to the random parameters $K_{m,1}$, $K_{m,4}$, $V_{\max,2}$, and $V_{\max,5}$. For other parameters, we assign the aforementioned nominal values and treat them as deterministic. The tuning parameter I is taken to be 0.48.

After the training is finished, we march forward for $n = 1,400$ steps with the initial condition $\mathbf{x}_0 = (0.22685145, 0.98369158, 0.87752945)$ and compute the mean and variance with a tensor product of five-point Gaussian quadrature. In Fig. 4.10, we present the approximated mean and variance. Given such long-time simulation, the approximation agrees with the reference.

For this example, the response curve of e_{3p} with respect to the tuning parameter I

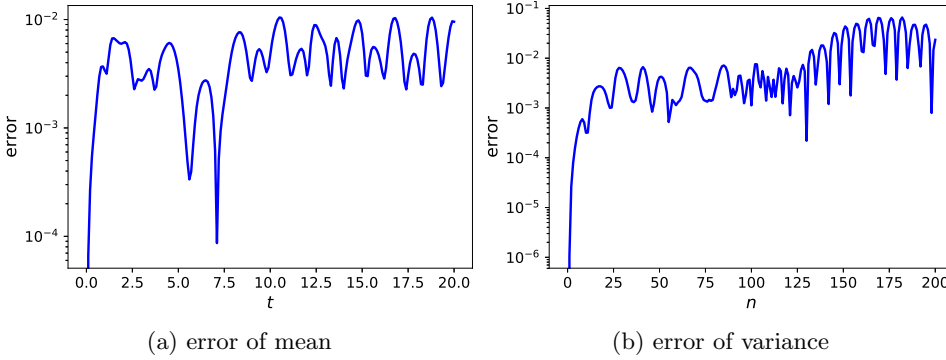
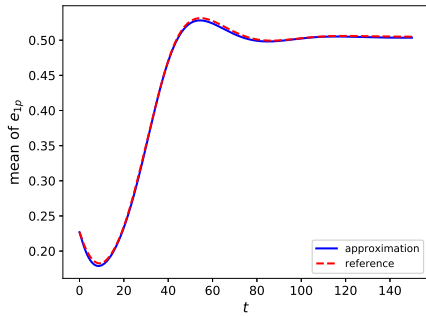


Fig. 4.9: Propagation of errors in the mean and variance of the solution to Example 3 with $\mathbf{x}_0 = (-1.193, -3.876)$.

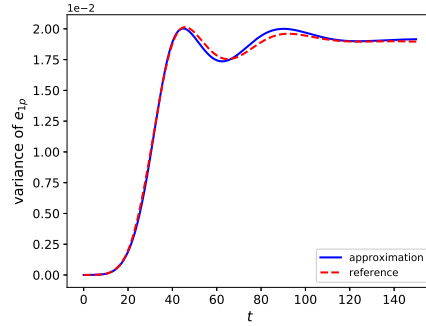
is of particular interest in practice. We examine such curve at the steady state of e_{3p} . To this end, we fix all the other parameters at their mean value and let I vary in $[0, 1.5]$. To reach the steady state, without solving the true governing equations for long time, we march the DNN model forward for 2000 steps as in (3.12). Fig. 4.11 presents the resulting response curve. There is a good agreement between the approximation and the reference response curve observed.

5. Conclusion. We presented a numerical framework for discovering unknown parameterized dynamical systems, using observational data and deep neural networks (DNN). The network structure is a modification to the residual network, which was shown to be effective to discover unknown deterministic dynamical systems in recent work [26]. Our method allows one to not only create accurate neural network model to approximate the unknown dynamics but also conduct efficient uncertainty quantification.

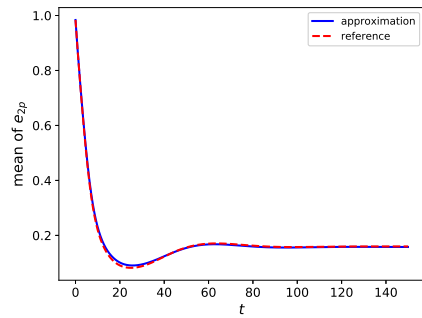
6. Acknowledgments. Sandia National Laboratories is a multi-mission laboratory managed and operated by National Technology and Engineering Solutions of Sandia, LLC., a wholly owned subsidiary of Honeywell International, Inc., for the U.S. Department of Energy’s National Nuclear Security Administration under contract DE-NA-0003525. The views expressed in the article do not necessarily represent the views of the U.S. Department of Energy or the United States Government.



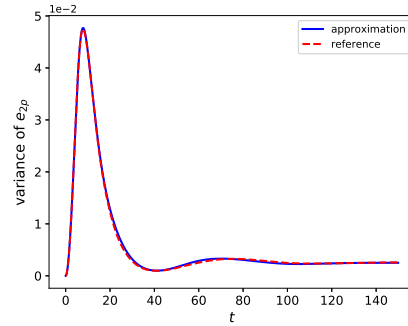
(a) mean of e_{1p}



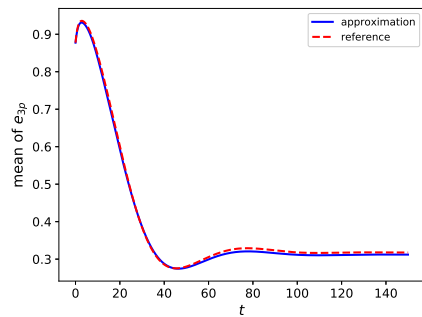
(b) variance of e_{1p}



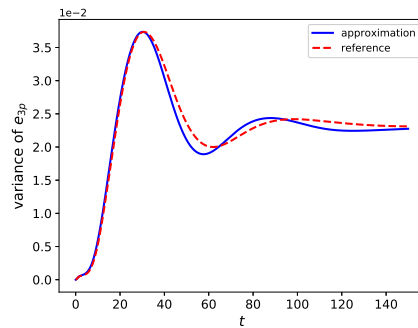
(c) mean of e_{2p}



(d) variance of e_{2p}



(e) mean of e_{3p}



(f) variance of e_{3p}

Fig. 4.10: Mean (left column) and variance (right column) of the solution to Example 4.

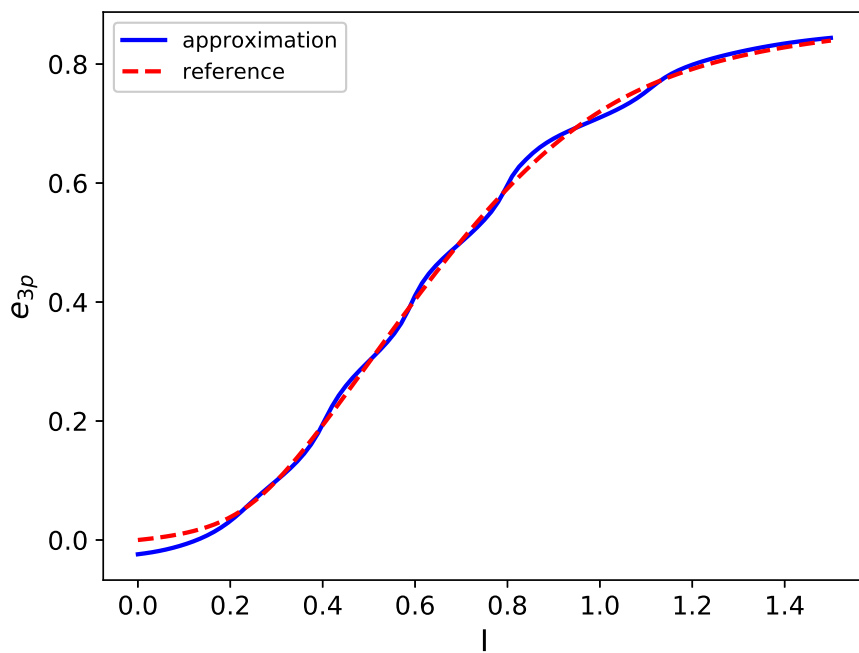


Fig. 4.11: Response curve of the steady state of e_{3p} with respect to I for Example 4.

REFERENCES

- [1] M. ABADI, A. AGARWAL, P. BARHAM, E. BREVDO, Z. CHEN, C. CITRO, G. S. CORRADO, A. DAVIS, J. DEAN, M. DEVIN, S. GHEMAWAT, I. GOODFELLOW, A. HARP, G. IRVING, M. ISARD, Y. JIA, R. JOZEFOWICZ, L. KAISER, M. KUDLUR, J. LEVENBERG, D. MANÉ, R. MONGA, S. MOORE, D. MURRAY, C. OLAH, M. SCHUSTER, J. SHLENS, B. STEINER, I. SUTSKEVER, K. TALWAR, P. TUCKER, V. VANHOUCKE, V. VASUDEVAN, F. VIÉGAS, O. VINYALS, P. WARDEN, M. WATTENBERG, M. WICKE, Y. YU, AND X. ZHENG, *TensorFlow: Large-scale machine learning on heterogeneous systems*, 2015, <https://www.tensorflow.org/>. Software available from tensorflow.org.
- [2] J. BONGARD AND H. LIPSON, *Automated reverse engineering of nonlinear dynamical systems*, Proc. Natl. Acad. Sci. U.S.A., 104 (2007), pp. 9943–9948.
- [3] S. L. BRUNTON, B. W. BRUNTON, J. L. PROCTOR, E. KAISER, AND J. N. KUTZ, *Chaos as an intermittently forced linear system*, Nature Communications, 8 (2017).
- [4] S. L. BRUNTON, J. L. PROCTOR, AND J. N. KUTZ, *Discovering governing equations from data by sparse identification of nonlinear dynamical systems*, Proc. Natl. Acad. Sci. U.S.A., 113 (2016), pp. 3932–3937.
- [5] X. CHEN, E.-J. PARK, AND D. XIU, *A flexible numerical approach for quantification of epistemic uncertainty*, Journal of Computational Physics, 240 (2013), pp. 211–224.
- [6] B. C. DANIELS AND I. NEMENMAN, *Automated adaptive inference of phenomenological dynamical models*, Nature Communications, 6 (2015).
- [7] B. C. DANIELS AND I. NEMENMAN, *Efficient inference of parsimonious phenomenological models of cellular dynamics using S-systems and alternating regression*, PloS One, 10 (2015), p. e0119821.
- [8] W. E, B. ENGQUIST, AND Z. HUANG, *Heterogeneous multiscale method: A general methodology for multiscale modeling*, Phys. Rev. B, 67 (2003), p. 092101.
- [9] M. GERRITSMAN, J.-B. VAN DER STEEN, P. VOS, AND G. KARNIADAKIS, *Time-dependent generalized polynomial chaos*, Journal of Computational Physics, 229 (2010), pp. 8333–8363.
- [10] R. GHANEM AND P. D. SPANOS, *Polynomial chaos in stochastic finite elements*, Journal of Applied Mechanics, 57 (1990), pp. 197–202.
- [11] D. GIANNAKIS AND A. J. MAJDA, *Nonlinear Laplacian spectral analysis for time series with intermittency and low-frequency variability*, Proc. Natl. Acad. Sci. U.S.A., 109 (2012), pp. 2222–2227.
- [12] R. GONZALEZ-GARCIA, R. RICO-MARTINEZ, AND I. G. KEVREKIDIS, *Identification of distributed parameter systems: A neural net based approach*, Comput. Chem. Eng., 22 (1998), pp. S965–S968.
- [13] J. HAN, A. JENTZEN, AND E. WEINAN, *Solving high-dimensional partial differential equations using deep learning*, Proceedings of the National Academy of Sciences, 115 (2018), pp. 8505–8510.
- [14] K. HE, X. ZHANG, S. REN, AND J. SUN, *Deep residual learning for image recognition*, in Proceedings of the IEEE conference on computer vision and pattern recognition, 2016, pp. 770–778.
- [15] J. HESTHAVEN AND S. UBBIALI, *Non-intrusive reduced order modeling of nonlinear problems using neural networks*, J. Comput. Phys., 363 (2018), pp. 55–78.
- [16] J. JAKEMAN, M. ELDRED, AND D. XIU, *Numerical approach for quantification of epistemic uncertainty*, Journal of Computational Physics, 229 (2010), pp. 4648–4663.
- [17] I. G. KEVREKIDIS, C. W. GEAR, J. M. HYMAN, P. G. KEVREKIDIS, O. RUNBORG, C. THEODOROPOULOS, ET AL., *Equation-free, coarse-grained multiscale computation: Enabling microscopic simulators to perform system-level analysis*, Commun. Math. Sci., 1 (2003), pp. 715–762.
- [18] D. P. KINGMA AND J. BA, *Adam: A method for stochastic optimization*, arXiv preprint arXiv:1412.6980, (2014).
- [19] I. E. LAGARIS, A. LIKAS, AND D. I. FOTIADIS, *Artificial neural networks for solving ordinary and partial differential equations*, IEEE transactions on neural networks, 9 (1998), pp. 987–1000.
- [20] Z. LONG, Y. LU, AND B. DONG, *Pde-net 2.0: Learning pdes from data with a numeric-symbolic hybrid deep network*, Journal of Computational Physics, 399 (2019), p. 108925.
- [21] Z. LONG, Y. LU, X. MA, AND B. DONG, *PDE-Net: learning PDEs from data*, arXiv preprint arXiv:1710.09668, (2017).
- [22] Z. LONG, Y. LU, X. MA, AND B. DONG, *PDE-net: Learning PDEs from data*, 80 (2018), pp. 3208–3216, <http://proceedings.mlr.press/v80/long18a.html>.
- [23] N. M. MANGAN, J. N. KUTZ, S. L. BRUNTON, AND J. L. PROCTOR, *Model selection for dy-*

- namiical systems via sparse regression and information criteria*, Proceedings of the Royal Society of London A: Mathematical, Physical and Engineering Sciences, 473 (2017).
- [24] B. PEHERSTORFER AND K. WILLCOX, *Data-driven operator inference for nonintrusive projection-based model reduction*, Computer Methods in Applied Mechanics and Engineering, 306 (2016), pp. 196–215.
- [25] A. PINKUS, *Approximation theory of the MLP model in neural networks*, Acta Numerica, 8 (1999), pp. 143–195.
- [26] T. QIN, K. WU, AND D. XIU, *Data driven governing equations approximation using deep neural networks*, Journal of Computational Physics, 395 (2019), pp. 620–635.
- [27] M. RAISSI, *Deep hidden physics models: Deep learning of nonlinear partial differential equations*, The Journal of Machine Learning Research, 19 (2018), pp. 932–955.
- [28] M. RAISSI, P. PERDIKARIS, AND G. E. KARNIADAKIS, *Machine learning of linear differential equations using gaussian processes*, Journal of Computational Physics, 348 (2017), pp. 683–693.
- [29] M. RAISSI, P. PERDIKARIS, AND G. E. KARNIADAKIS, *Multistep neural networks for data-driven discovery of nonlinear dynamical systems*, arXiv preprint arXiv:1801.01236, (2018).
- [30] D. RAY AND J. HESTHAVEN, *An artificial neural network as a troubled-cell indicator*, J. Comput. Phys., 367 (2018), pp. 166–191.
- [31] D. RAY AND J. S. HESTHAVEN, *Detecting troubled-cells on two-dimensional unstructured grids using a neural network*, Journal of Computational Physics, 397 (2019), p. 108845.
- [32] S. H. RUDY, J. N. KUTZ, AND S. L. BRUNTON, *Deep learning of dynamics and signal-noise decomposition with time-stepping constraints*, Journal of Computational Physics, 396 (2019), pp. 483–506.
- [33] P. J. SCHMID, *Dynamic mode decomposition of numerical and experimental data*, Journal of fluid mechanics, 656 (2010), pp. 5–28.
- [34] M. SCHMIDT AND H. LIPSON, *Distilling free-form natural laws from experimental data*, Science, 324 (2009), pp. 81–85.
- [35] M. D. SCHMIDT, R. R. VALLABHAJOSYULA, J. W. JENKINS, J. E. HOOD, A. S. SONI, J. P. WIKSWO, AND H. LIPSON, *Automated refinement and inference of analytical models for metabolic networks*, Physical Biology, 8 (2011), p. 055011.
- [36] S. Y. SHVARTSMAN, M. HAGAN, A. YACCOUB, P. DENT, H. WILEY, AND D. A. LAUFFENBURGER, *Autocrine loops with positive feedback enable context-dependent cell signaling*, American Journal of Physiology-Cell Physiology, 282 (2002), pp. C545–C559.
- [37] J. SIRIGNANO AND K. SPILIOPOULOS, *Dgm: A deep learning algorithm for solving partial differential equations*, Journal of Computational Physics, 375 (2018), pp. 1339–1364.
- [38] A. STUART AND A. R. HUMPHRIES, *Dynamical Systems and Numerical Analysis*, vol. 2, Cambridge University Press, 1998.
- [39] G. SUGIHARA, R. MAY, H. YE, C. HSIEH, E. DEYLE, M. FOGARTY, AND S. MUNCH, *Detecting causality in complex ecosystems*, Science, 338 (2012), pp. 496–500.
- [40] R. TIBSHIRANI, *Regression shrinkage and selection via the lasso*, Journal of the Royal Statistical Society. Series B (Methodological), (1996), pp. 267–288.
- [41] G. TRAN AND R. WARD, *Exact recovery of chaotic systems from highly corrupted data*, Multi-scale Model. Simul., 15 (2017), pp. 1108–1129.
- [42] R. K. TRIPATHY AND I. BILIONIS, *Deep uq: Learning deep neural network surrogate models for high dimensional uncertainty quantification*, Journal of Computational Physics, 375 (2018), pp. 565–588.
- [43] H. U. VOSS, P. KOLODNER, M. ABEL, AND J. KURTHS, *Amplitude equations from spatiotemporal binary-fluid convection data*, Phys. Rev. Lett., 83 (1999), p. 3422.
- [44] E. WEINAN AND B. YU, *The deep ritz method: a deep learning-based numerical algorithm for solving variational problems*, Communications in Mathematics and Statistics, 6 (2018), pp. 1–12.
- [45] K. WU, T. QIN, AND D. XIU, *Structure-preserving method for reconstructing unknown hamiltonian systems from trajectory data*, arXiv preprint arXiv:1905.10396, (2019).
- [46] K. WU AND D. XIU, *Numerical aspects for approximating governing equations using data*, J. Comput. Phys., 384 (2019), pp. 200–221.
- [47] K. WU AND D. XIU, *Data-driven deep learning of partial differential equations in modal space*, J. Comput. Phys., 408 (2020), p. 109307.
- [48] D. XIU AND G. E. KARNIADAKIS, *The wiener-askay polynomial chaos for stochastic differential equations*, SIAM journal on scientific computing, 24 (2002), pp. 619–644.
- [49] Y. YANG AND P. PERDIKARIS, *Adversarial uncertainty quantification in physics-informed neural networks*, Journal of Computational Physics, 394 (2019), pp. 136–152.
- [50] H. YE, R. J. BEAMISH, S. M. GLASER, S. C. H. GRANT, C. HSIEH, L. J. RICHARDS, J. T.

- SCHNUTE, AND G. SUGIHARA, *Equation-free mechanistic ecosystem forecasting using empirical dynamic modeling*, Proc. Natl. Acad. Sci. U.S.A., 112 (2015), pp. E1569–E1576.
- [51] Y. ZHU AND N. ZABARAS, *Bayesian deep convolutional encoder–decoder networks for surrogate modeling and uncertainty quantification*, Journal of Computational Physics, 366 (2018), pp. 415–447.
- [52] Y. ZHU, N. ZABARAS, P.-S. KOUTSOURELAKIS, AND P. PERDIKARIS, *Physics-constrained deep learning for high-dimensional surrogate modeling and uncertainty quantification without labeled data*, Journal of Computational Physics, 394 (2019), pp. 56–81.